Materials Transactions, Vol. 67, No. 9 (2026) pp. 1621 to 1630

TECHNICAL ARTICLE

Effect of Lattice Parameters of Master Pattern on EBSD Indexing via Pattern Matching*1

Tomotaka Hatakeyama*2 and Kota Sawada

Research Center for Structural Materials, National Institute for Materials Science, Tsukuba 305-0047, Japan

The effects of the lattice parameter of the simulated master pattern and the EBSD pattern resolution for indexing of EBSD patterns via pattern matching (Spherical Indexing) were investigated using annealed austenitic steel. A larger deviation from the accurate lattice parameter in the master pattern resulted in a larger deviation from the true crystallographic orientation. Poorer EBSD pattern resolution resulted in a lower angular resolution, especially near the grain boundary, and increased kernel average misorientation (KAM) values. These results suggest that accurate lattice parameter and higher pattern resolution are required for Spherical Indexing to achieve a better angular resolution. Nevertheless, Spherical Indexing using a master pattern with a 15% deviation from the accurate lattice parameter and EBSD patterns with a binning of 8×8 provided a better angular resolution than traditional indexing using the Hough transformation of EBSD patterns without binning (binning of 1×1). This indicates that Spherical Indexing is an excellent indexing procedure in terms of angular resolution, which is robust for the lattice parameter of the master pattern and EBSD pattern resolution. [doi:10.2320/matertrans.MT-M2026070]

(Received May 28, 2026; Accepted June 15, 2026; Published July 3, 2026)

Keywords: *electron backscattered diffraction, pattern matching, Spherical Indexing, misorientation, binning, lattice parameter*

1. Introduction

In electron backscatter diffraction (EBSD), an electron beam is directed onto a highly tilted crystalline specimen to generate an EBSD pattern. The crystal orientation is determined by collecting this pattern and analyzing the positional relationships of the bands (which correspond to the crystal planes) within it. When the measurement points are arranged in a grid, the resulting map data of crystal orientations can be analyzed to extract a wide range of microstructural factors, such as texture, grain boundary character, and local misorientation between adjacent measurement points. Consequently, EBSD has become an indispensable technique for the microstructural analysis of metallic materials in recent years [1].

Commercial EBSD software automates the processes of pattern collection, band detection, and indexing. The Hough transformation is commonly used for automatic band detection on pattern images. The Hough transformation is a simple mathematical operation that converts lines into points [2], making it well-suited for fast automatic band detection. The crystal orientation was determined by comparing the angular relationships of the bands detected by the Hough transformation with those of crystal planes in a predefined crystal structure [3].

However, factors such as the width and contrast of the bands introduce unavoidable random measurement errors of approximately 1° in the bands detected by the Hough transformation compared with the actual orientation [4]. While such errors are negligible when evaluating texture or grain boundary character, they can pose significant issues in cases where, for example, one aims to estimate small plastic strain amounts of a few percent from local misorientation for creep damage assessment [5–7].

Recent advances in EBSD pattern simulation technology and computational capabilities have led to the development of a new method called Spherical Indexing, which performs indexing by pattern matching between master patterns generated through simulation and patterns obtained experimentally [8, 9]. This approach is expected to enable indexing even when part of the pattern is missing by using features visible in the limited pattern and to achieve significantly improved angular resolution owing to the reduced measurement error.

When indexing cubic crystals using the Hough transformation, only the crystal structure needs to be specified because the angular relationships between the crystal planes do not depend on the lattice constant. In contrast, when using pattern matching, it is necessary to specify both the crystal structure and lattice constant when creating the master pattern. In such cases, the lattice constant data of pure metals from databases are applied to alloy specimens with unknown lattice constants for convenience. However, the reliability of the indexing results under these circumstances is unclear. Therefore, it is essential to quantitatively understand the effect of the lattice constant error in the master pattern on the indexing results during pattern matching and to analyze the data with full awareness of any possible influences. In this study, we investigated the influence of the lattice constant of the master pattern on the indexing results of EBSD using pattern matching techniques.

2. Experimental Procedures

The test material was a 25Cr-20Ni-Nb-N steel tube (KA-SUS310J1TB) that was solution-treated at 1503 K and then water-cooled. The chemical compositions of the steel are listed in Table 1 [10, 11]. The lattice constant was measured by X-ray diffraction (XRD: Rigaku SmartLab) using samples that were mirror-polished with waterproof sandpaper, diamond paste, and colloidal silica on a buff. Cu-Kα radiation was used for the X-rays. The same sample was also used to

*1This Paper was Originally Published in Japanese in J. Japan Inst. Met. Mater. **90** (2026) 17–26.
*2Corresponding author, E-mail: hatakeyama.tomotaka@nims.go.jp

Table 1 Requirement [10] and chemical composition of 25Cr–20Ni–Nb–N steel (mass%) [11].

	C	Si	Mn	P	S	Ni	Cr	Nb	N
Requirement	≤0.10	≤1.50	≤2.00	≤0.030	≤0.030	17.00–23.00	23.00–27.00	0.20–0.60	0.15–0.35
TEA	0.06	0.41	1.25	0.018	0.001	19.84	24.60	0.46	0.272

Table 2 EBSD conditions performed in this study.

Binning	Resolution	Scan speed (fps)	File size (GB)
1×1	1392×1040	23	27.5
2×2	696×520	44	6.9
4×4	348×260	77	1.7
8×8	174×130	123	0.4

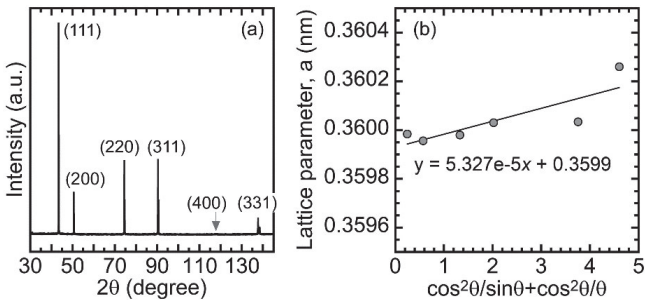

Fig. 1 (a) XRD profiles of the sample and (b) lattice constant calculation method by Nelson-Riley function.

collect EBSD patterns using an EBSD system (EDAX Digiview) installed on a scanning electron microscope (ZEISS Auriga Laser). The measurement area was 500 × 500 µm with a step size of 2.5 µm. The binning of the patterns was varied according to Table 2, and maps were obtained in nearly the same field of view under the four different conditions. The smaller the binning, the slower the measurement speed and the larger the file size required. Based on the lattice constant a for the 25Cr-20Ni-Nb-N steel obtained by XRD, six master patterns were simulated using dynamical diffraction theory [12, 13] with OIM Analysis 9 (EDAX) and OIM Matrix (EDAX), assuming the crystal structure to be face-centered cubic (fcc, space group: Fm-3m), and the lattice constants to be a, 1.01a, 1.03a, 1.05a, 1.10a, and 1.15a. Spherical Indexing was then performed for pattern matching and re-indexing.

3. Results and Discussion

The XRD profile of the sample is presented in Fig. 1(a). The lattice constants calculated from the positions of each peak were plotted against the Nelson-Riley function [14], as shown in Fig. 1(b), and by extrapolating to $\theta = \pi/2$, the lattice constant of the sample was determined to be 0.3599 nm. Figure 2 schematically illustrates how the EBSD pattern generated by the diffraction of electron beams near the surface of the specimen is projected onto a fluorescent screen [15]. The EBSD pattern results from the incident electron beam scattering near the sample surface, where the scattered electrons diffract at the crystal planes and emerge from the sample surface. The pattern projected onto the screen was captured using a CCD or CMOS camera.

When the interplanar spacing of the (hkl) plane is denoted as d_{hkl} and the electron beam wavelength as λ, diffraction occurs at an angle θ according to Bragg's law, as expressed in eq. (1).

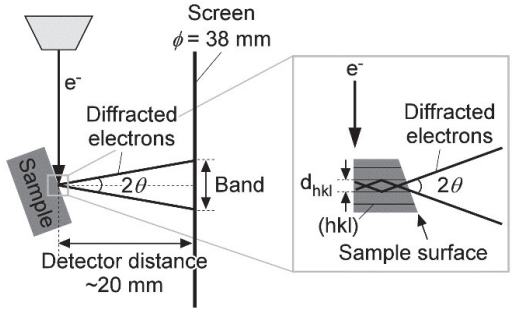

Fig. 2 Geometry of the sample, diffracted electrons, and screen in SEM chamber.

$$\lambda = 2d_{hkl}\sin\theta \tag{1}$$

At this time, the electron beams diffracted in the vertical direction were projected onto the screen, forming bands in the EBSD pattern. Therefore, the width of the bands in the EBSD pattern depends on the diffraction angle, θ. According to eq. (1), as the accelerating voltage increases, λ becomes smaller; thus, even if d_{hkl} remains the same, θ becomes smaller, resulting in narrower bands. Similarly, as the interplanar spacing increased, θ decreased, and the bands became narrower. Here, when the distance between the sample surface and the screen is L, the bandwidth w can be geometrically determined using eq. (2).

$$w = 2L\tan\theta \sim 2L\sin\theta \ (\theta \ll 1) \tag{2}$$

From eqs. (1) and (2), if the interplanar spacing changes from d_0 to d_1, and the corresponding bandwidths are w_0 and w_1, respectively, eq. (3) can be obtained.

$$w_1 = w_0 d_0 / d_1 \tag{3}$$

In other words, there is an inverse relationship between bandwidth and interplanar spacing. In this study, as shown in Table 3, six types of master patterns were created on the side

Table 3 Lattice parameters of the master patterns prepared in this study and the deviation from the true lattice parameter.

Deviation (%)	Lattice parameter, a (nm)
0	0.3599
+1	0.3635
+3	0.3707
+5	0.3779
+10	0.3959
+15	0.4139

with a larger lattice constant (i.e., the side with a smaller bandwidth), with the lattice constant increased by up to 15%. The upper limit for the lattice constant error, set at 15%, was determined by considering the Hume-Rothery rule [16].

Figure 3 shows the master pattern of fcc with a lattice constant of (a) $a = 0.3599$ nm (lattice constant determined by XRD) and (b) $a = 0.4139$ nm (lattice constant determined by XRD + 15%). Figures 3(c)–(d) and (e)–(f) show magnified views of the center and right end of each master pattern, respectively. The changes in brightness values along the arrows in Figs. 3(c)–(d) and (e)–(f) are shown in Figs. 3(g) and (h), respectively. It is evident that the contrast within the bands of the master patterns changes depending on the lattice constants. Furthermore, as indicated by the arrow in the center of Fig. 3(h), it can be confirmed that in the master pattern with a larger lattice constant $a = 0.4139$ nm, the bandwidth becomes narrower. However, the central positions of the bands and the positions of the zone axes where the bands cross do not change with the lattice constant. This is because the positions of the bands in the EBSD pattern are determined by the geometric relationship between the crystal planes and the screen [17].

In this study, in addition to the error in the lattice constant, EBSD measurements were performed with four types of binning to investigate the effect of the EBSD pattern resolution, as shown in Table 2. Figure 4 shows the EBSD patterns obtained for each binning. From the enlarged views in the lower section, it can be seen that the larger the binning, the coarser the pattern. In this case, the number of pixels along the width of a single band change. Taking as an example the band corresponding to the (202) detected almost horizontally in the pattern of Fig. 4, as shown in Figs. 4(e)–(h) and Table 4, when binning is 1×1, one band is represented by 35 pixels, whereas with 8×8 binning, it is represented by 4 pixels. Therefore, the change in the lattice constant (interplanar spacing) necessary for the band width to change by one pixel is estimated to be $1 \div 35 = 2.9\%$ for 1×1 binning and $1 \div 4 = 25\%$ for 8×8 binning. From this, it can be inferred that smaller binning is more sensitive to changes in the lattice constant of the master pattern.

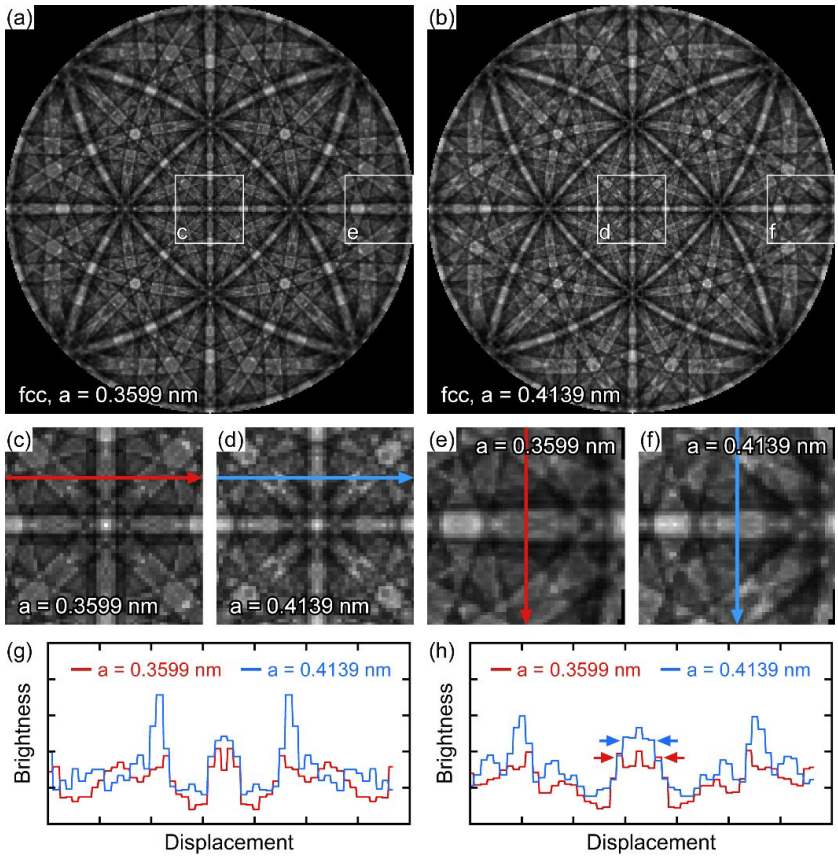

Fig. 3 Simulated EBSD master patterns for fcc with a lattice parameter of (a) 0.3599 nm and (b) 0.4139 nm. (c)–(f) Enlarged master patterns from the square box labeled as "c", "e" in (a), "d", and "f" in (b), and (g) and (h) brightness along the lines in (c), (d) and (e), (f), respectively. (online color)

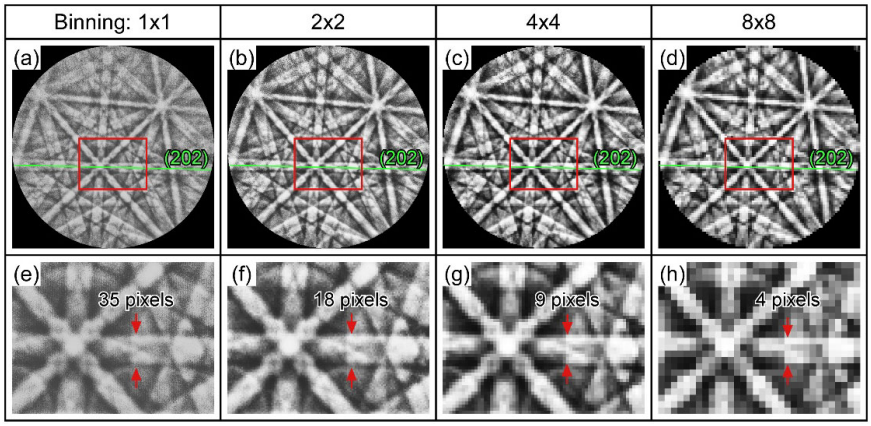

Fig. 4 EBSD patterns obtained from the binning sizes of (a) (e) 1 × 1, (b) (f) 2 × 2, (c) (g) 4 × 4, and (d) (h) 8 × 8. (online color)

Table 4 Number of pixels along a band for (202) and the change in lattice parameter when the band width is increased by one pixel in each binning size.

Binning	Number of pixels along a band for (202)	Change in Lattice parameter when the band width is increased by one pixel (%)
1×1	35	2.9
2×2	18	5.6
4×4	9	11.1
8×8	4	25.0

Table 5 Calculations to obtain the change in crystallographic orientation (θ) required to detect the change in the position of the band near the center of the screen as a shift of 1 pixel.

Binning	Screen diameter (mm)	Number of pixels along Y axis	Pixel size (μm)	tanθ	θ (deg.)
1×1	38	1040	36.5	0.00183	0.105
2×2	38	520	70.4	0.00352	0.202
4×4	38	260	146.2	0.00731	0.419
8×8	38	130	292.3	0.01462	0.838

When a horizontal band is detected near the center of the pattern, such as the (202) in Fig. 4, shifts by one pixel in the Y direction, the change in orientation (crystal rotation) can be geometrically calculated using eq. (4) in Fig. 2. The rotation angle (θ) was determined by the number of pixels in the Y-direction of the pattern image defined by binning, the diameter of the screen, and the distance between the sample surface and the screen ($L = 20$ mm).

$$L \tan\theta = \text{Pixel size} = \frac{\text{Number of pixels along Y axis}}{\text{Screen diameter}} \quad (4)$$

The orientation change that occurs when the central band shifts by one pixel in each binning was estimated to be approximately 0.1° for 1 × 1 binning and approximately 0.8° for 8 × 8 binning, as shown in Table 5. This suggests that smaller binning results in a higher angular resolution for indexing.

When performing pattern matching using Spherical Indexing, each measurement point is assigned a value called the Spherical Confidence Index (SCI), ranging from 0 to 1, representing the degree of correlation (confidence index) between the experimentally obtained EBSD pattern and the master pattern. Figure 5 presents the SCI maps obtained by Spherical Indexing using the master patterns generated with the six different lattice constants listed in Table 3, for the 1 × 1 binning pattern, which is expected to be the most sensitive to changes in the lattice constant of the master pattern as shown in Table 4. There were differences in the SCI between the crystal grains, but little variation within each grain. The specimen used in this study was in a solution-

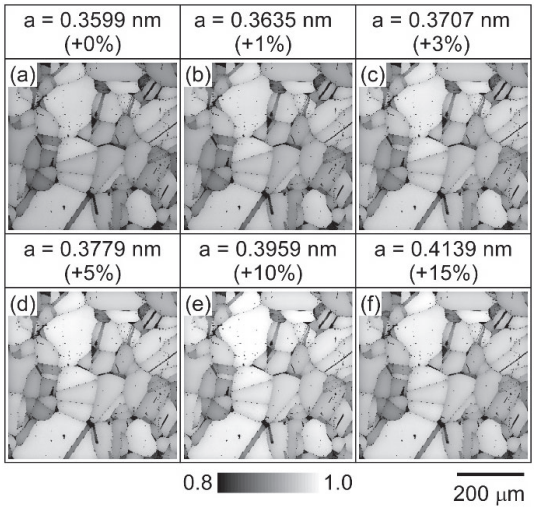

Fig. 5 SCI map of obtained by the binning size of 1 × 1 by the Spherical indexing with lattice parameters of the master pattern (a) 0.3599, (b) 0.3635, (c) 0.3707, (d) 0.3779, (e) 0.3959, and (f) 0.4139 nm.

treated condition, and because clear patterns were obtained, high SCI values of 0.8 or above were achieved throughout the entire field of view. This indicates that accurate indexing was performed regardless of the lattice constant of the master pattern.

Figure 6(a) shows the relationship between the lattice constant of the master pattern and the average SCI of the measurement area when the binning is 1 × 1. The average SCI is highest when the master pattern created with $a = 0.3959$ nm (lattice constant obtained by XRD +10%) is used, and it decreases as the difference from 0.3959 nm increases. The average SCI values for $a = 0.3779$ nm (+5%) and 0.4139 nm (+15%), both with a 5% difference from 0.3959 nm, were nearly identical. The same tendency was observed in the SCI histograms shown in Fig. 6(b). The results of Spherical Indexing using master patterns with $a = 0.3599$ nm and 0.3959 nm for the EBSD pattern of the specimen with binning 1 × 1 shown in Fig. 6(c) are presented in Fig. 6(d) and (e), respectively. The SCI values were 0.885 and 0.931, respectively. Enlarged views of the central boxed area in Fig. 6(c)–(e) are shown in Fig. 6(f)–(h). The brightness variation along the arrow in the figure is shown in Fig. 6(l). It can be seen that the band width of the EBSD pattern of the specimen is better reproduced by the master pattern with $a = 0.3599$ nm. However, in the enlarged views of the lower boxed area in Fig. 6(c)–(e), shown in Fig. 6(i)–(k), the locations indicated by arrows suggest that the fine contrast within the bands is better reproduced by the master pattern with $a = 0.3959$ nm. Therefore, as a result of pattern matching that includes fine contrast within the bands, it is presumed that the average SCI is the highest at

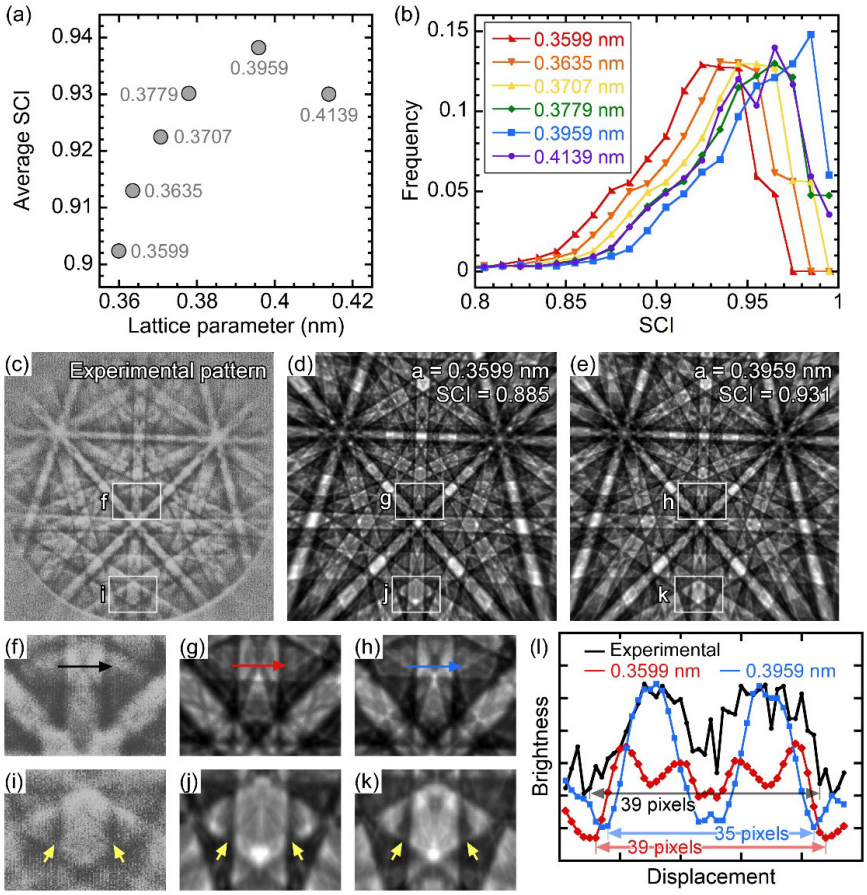

Fig. 6 (a) Relationship between lattice parameter of the master pattern and average SCI value and (b) effect of lattice parameter of master pattern on histograms of SCI values with a binning of 1 × 1. (c) An example of experimentally obtained EBSD pattern with a binning of 1 × 1, matched master patterns with a lattice parameter of (d) 0.3599 and (e) 0.3959 nm, (f)–(k) enlarged patterns from the boxes in (c)–(e), and brightness along the lines in (f)–(h). (online color)

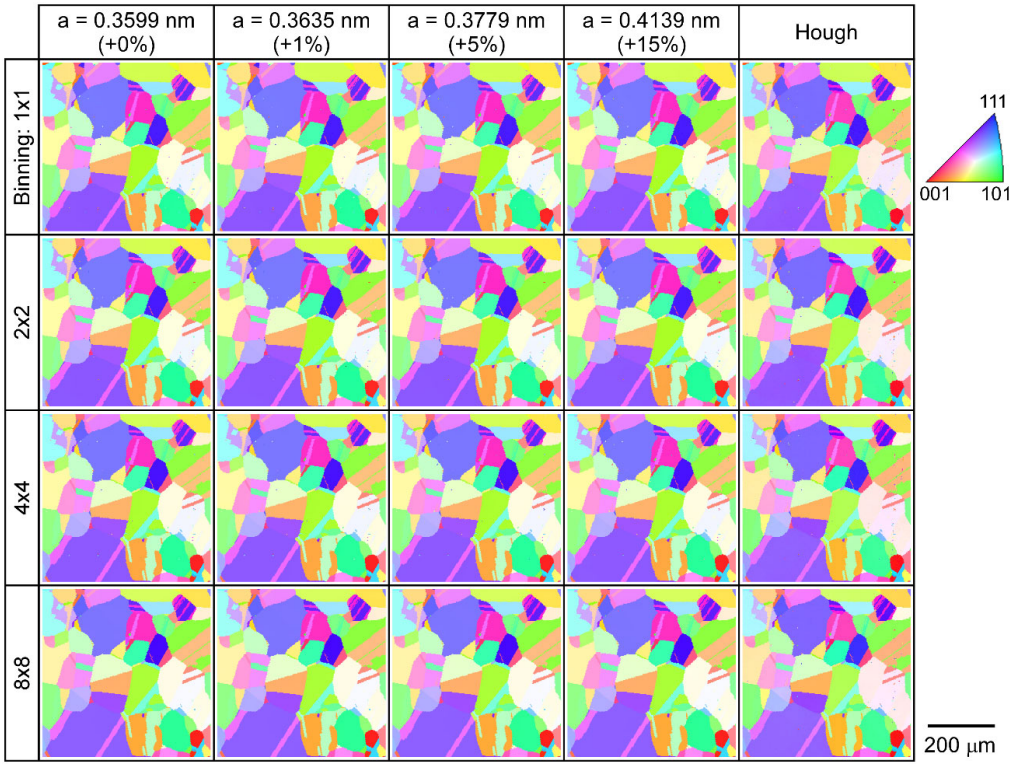

Fig. 7 Inverse pole figure (IPF) maps obtained by the binning sizes of 1 × 1 to 8 × 8 by the Spherical indexing with several lattice parameters of the master pattern and Hough indexing. (online color)

$a = 0.3959$ nm. In contrast, the crystal orientation determined by pattern matching is considered to be the most accurate when the band width is well reproduced, that is, at $a = 0.3599$ nm.

Figure 7 shows the Inverse Pole Figure (IPF) maps obtained by Spherical Indexing and Hough transformation using master patterns created with various lattice constants for each binning. The influence of the pattern resolution and master pattern lattice constant was not evident from the IPF maps.

As described above, regardless of the SCI shown in Fig. 5 and 6, the crystal orientation obtained by Spherical Indexing using a master pattern created with the lattice constant determined by XRD ($a = 0.3599$ nm) is considered to be the closest to the actual crystal orientation. Therefore, for each Binning, based on the pattern at each measurement point, the orientation difference was calculated between the crystal orientation obtained by Spherical Indexing with $a = 0.3599$ nm and those obtained from master patterns with lattice constants having 1–15% error, using the same pattern with both Spherical Indexing and the Hough transformation. The results are shown as disorientation maps in Fig. 8.

When indexing with Spherical Indexing, larger errors in the lattice constant resulted in greater orientation differences. However, even with a 15% difference in the lattice constant, the orientation difference at most measurement points was less than 0.1°, which is very small. The effect of binning was not observed in the disorientation maps. The orientation difference observed at this time was approximately the same for each grain, suggesting that within the same grain with similar patterns, pattern matching consistently produced a comparable orientation difference. However, when indexed using the Hough transformation, orientation differences of up to approximately 2° were observed.

The relationship between the average orientation difference across the entire field of view (shown in Fig. 8) and the error in the lattice constant of the master pattern (Δa) used for Spherical Indexing is shown in Fig. 9. The larger the Δa, the greater the average orientation difference. However, even when Δa was 15%, the average orientation difference was approximately 0.02–0.03°, indicating that the influence of the master pattern lattice constant on the orientation determination accuracy by Spherical Indexing was small.

As shown in Table 4, if the binning is 1 × 1, a difference of approximately 3% in the lattice constant appears as a band width in the pattern. However, in Spherical Indexing, orientations are determined not by a single bandwidth but by matching the entire acquired pattern. As shown in Fig. 3(a) and (b), in the EBSD patterns, neither the band center position nor the position of the zone axis where the bands intersect is affected by the lattice constant [17]. Therefore, it is presumed that the effect of the master pattern lattice constant (band width) on the orientation determination accuracy was small.

However, the larger the binning, the smaller the average orientation difference. In other words, as suggested in Table 5, the larger binning resulted in less sensitivity to the changes in the master pattern lattice constant. However, the difference in the average orientation difference between Binning 1 × 1 and 8 × 8 was as small as approximately 0.01°, even when Δa was 15%.

Figure 10 shows the frequency distribution of the orientation differences obtained by the Hough transformation, as indicated in Fig. 8. Comparing the Hough transformation

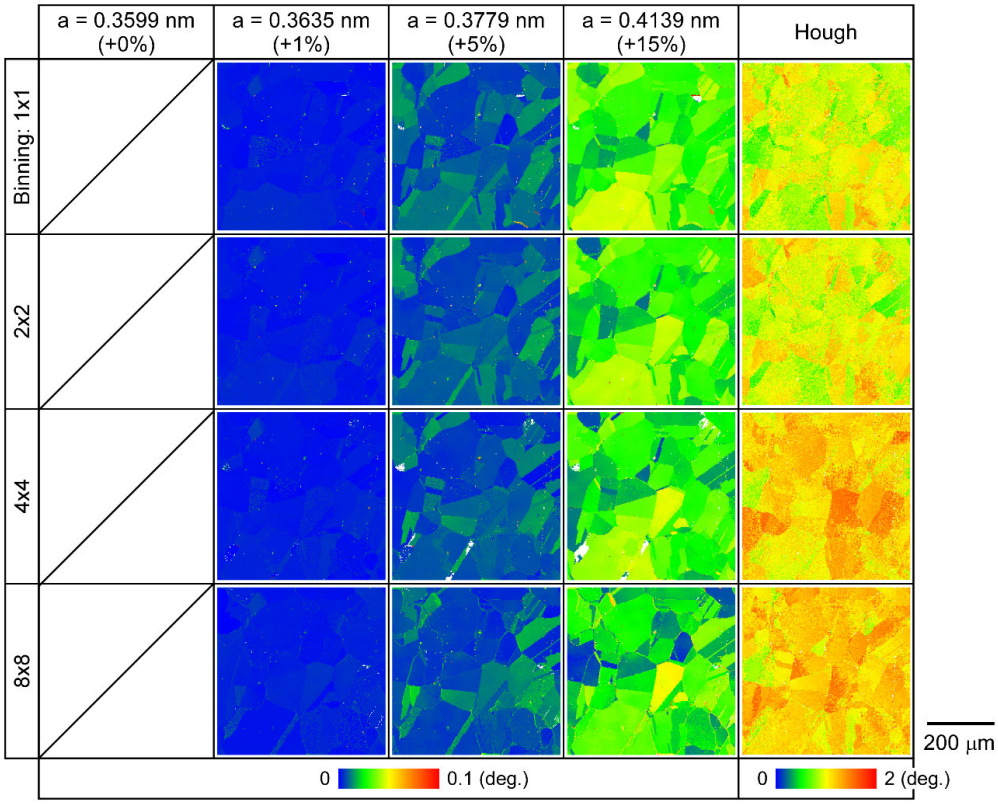

Fig. 8 Disorientation from the crystallographic orientation obtained by the Spherical Indexing with a lattice parameter of 0.3599 nm calculated against the binning sizes of 1 × 1 to 8 × 8 by the Spherical indexing with several lattice parameters of the master pattern and Hough indexing. (online color)

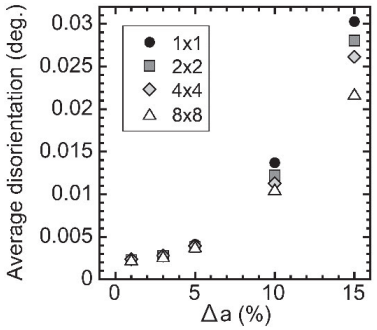

Fig. 9 Relationship between the deviation of lattice parameter of master pattern (Δa) and average disorientation.

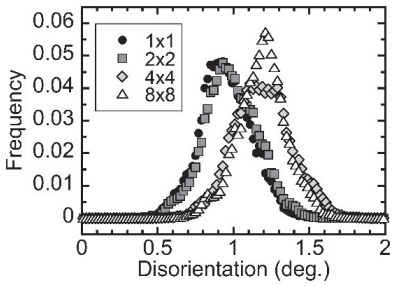

Fig. 10 Histograms of the disorientation between the crystallographic orientation obtained by the Spherical Indexing with a lattice parameter of 0.3599 nm and that obtained by Hough indexing.

with Spherical Indexing using accurate lattice constants, it was found that an orientation difference of approximately $1 \pm 0.2°$ on average arose. This value is larger than the orientation differences between the orientations determined by Spherical Indexing, as shown in Fig. 9, indicating that this can be attributed to errors from the Hough transformation. In other words, compared to the Hough transformation, Spherical Indexing allows the determination of orientations with higher accuracy.

The orientation determination accuracy discussed based on Figs. 8–10 is a relative evaluation, assuming that the crystal orientations determined by Spherical Indexing with accurate lattice constants are correct. However, because the twin boundary in fcc crystals has an orientation difference of 60°, the reliability of the orientation measurements can also be evaluated in absolute terms. Therefore, the orientation differences across both sides of more than 40 twin boundaries per field of view were measured, and deviations from 60° were calculated.

Figures 11(a)–(d) present histograms of the deviations from 60° in the orientation difference at the twin boundaries, obtained from the indexing results by Spherical Indexing and the Hough transformation using master patterns with lattice constants of 0.3599 nm or 0.4139 nm and binning from 1 × 1 to 8 × 8. Figure 11(e) shows the average of these deviations. Error bars indicate standard deviation. According to the results obtained by Spherical Indexing, no influence of binning or the lattice constants of the master pattern was observed. In contrast, when comparing the average orientation differences in Spherical Indexing and the Hough transformation, the Hough transformation values were approximately three times larger. This further confirms that Spherical Indexing determines orientations with high accuracy.

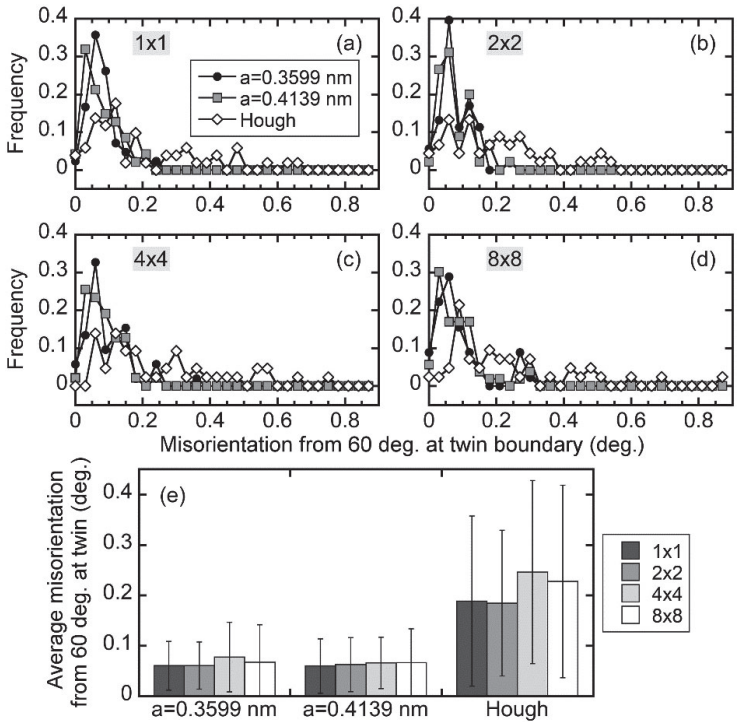

Fig. 11 Histogram of the misorientation from 60 deg. at twin boundary with a binning size of (a) 1 × 1, (b) 2 × 2, (c) 4 × 4, and (d) 8 × 8, and (e) average misorientation from 60 deg. at twin boundary.

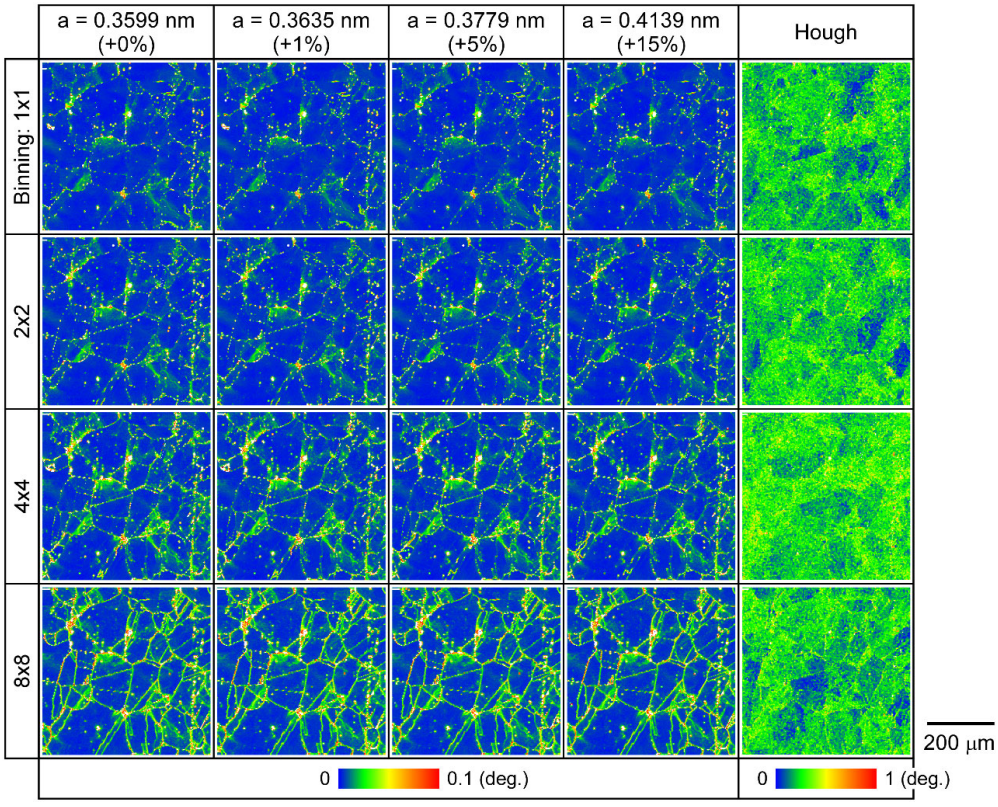

Fig. 12 Kernel average misorientation (KAM) maps obtained by the binning sizes of 1 × 1 to 8 × 8 by the Spherical indexing with several lattice parameters of the master pattern and Hough indexing. (online color)

Figure 12 shows the Kernel Average Misorientation (KAM) maps obtained by Spherical Indexing and Hough transformation using master patterns with various lattice constants for each binning. The KAM is defined as the average orientation difference between a measurement point and its six neighboring points. If a neighboring measurement point crossed a grain boundary, it was excluded from the calculation.

In the resulting KAM maps, when binning was held constant, no effect of the master pattern lattice constants was

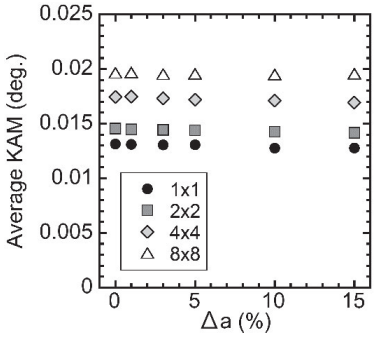

Fig. 13 Relationship between the deviation of lattice parameter of master pattern (Δa) and average KAM.

observed. In contrast, the KAM map changed with binning: the larger the binning, the higher the KAM, particularly near the grain boundaries. However, even at a binning of 8×8, the KAM near the grain boundaries was less than 0.1° for most measurement points.

Binning affects the file size as well as the processing speed of the measurement and re-indexing; thus, in practice, larger binning is easier to handle. The reason why the measurement results change with binning, as shown in Fig. 12, is unknown; however, because binning was shown to possibly influence local orientation difference parameters, such as KAM in Spherical Indexing, it is considered necessary to select appropriate binning according to the microstructural parameter to be evaluated. Compared with Spherical Indexing, the KAM values in the Hough transformation were significantly higher. This is because the measurement errors shown in Fig. 10 were added to the orientation differences between adjacent measurement points.

The relationship between the average KAM shown in Fig. 12 and the error (Δa) in the lattice constant of the master pattern used for Spherical Indexing is presented in Fig. 13. The KAM values obtained for each binning remained constant, regardless of Δa. As shown in Fig. 9, the crystal orientation obtained by Spherical Indexing changed depending on the lattice constant of the master pattern. Furthermore, within the same crystal grain, similar degrees of disorientation were consistently reproduced using pattern matching. This suggests that when the lattice constant of the master pattern changed, the indexing by pattern matching was performed such that the adjacent measurement points experienced crystal rotations in the same direction, resulting in no change in the KAM representing the local orientation difference between measurement points.

Because the test material used here was as-solution-treated, the orientation difference within the grains was small, and the average KAM was nearly zero. In other words, the average KAM obtained here can be considered to correspond to the orientation determination accuracy (angular resolution) of Spherical Indexing. As estimated from Table 5, the smaller the binning, the higher the angular resolution, resulting in a lower average KAM value. In contrast, the average KAM values were significantly smaller than those estimated in Table 5. The estimation from Table 5 suggests that the orientation accuracy is proportional to the length of one side of a pixel, and with 1×1 binning, it was assumed to have approximately eight times the orientation accuracy of 8×8 binning. However, the average KAM for 8×8 binning was only approximately 1.5 times that of 1×1 binning, indicating that sufficient orientation accuracy can be attained even with 8×8 binning.

In Spherical Indexing, indexing is performed not only based on the band width, which depends on the lattice constant, but also by pattern matching that includes the angular relationship between bands and the position of the zone axis, which does not depend on the lattice constant. Therefore, this is an excellent method for robustly and accurately determining the crystal orientation, regardless of the master pattern's lattice constant or the pattern's resolution. In other words, it was found that lattice constant errors of a few percent due to alloying have almost no effect on the indexing accuracy of Spherical Indexing, and there is no problem using a master pattern created from the lattice constant of a pure metal in the database.

4. Conclusions

(1) We investigated the effects of the lattice constant of the master pattern and the resolution of the EBSD pattern on the indexing method (Spherical Indexing) for EBSD patterns, which utilizes pattern matching with simulated master patterns.
(2) The greater the error in the lattice constant of the master pattern, the larger the deviation from the true crystal orientation. Therefore, it is necessary to accurately measure the lattice constant if one wishes to precisely determine the orientation differences between crystal grains.
(3) When the resolution of the EBSD pattern was low, the KAM near the grain boundaries increased. Thus, when evaluating minute orientation changes near grain boundaries as KAM, it is desirable to use high-resolution EBSD patterns.
(4) The orientation determination accuracy of Spherical Indexing outperformed that of the conventional Hough transformation-based method, even when the master pattern's lattice constant error was large or the EBSD pattern had a low resolution. This is presumably because the positional relationship of the zone axes does not change even if the lattice constant does, demonstrating that Spherical Indexing is a robust indexing method with respect to the lattice constant and pattern resolution.
(5) This study was conducted using solution-treated material. A future challenge is the verification of significantly deformed materials, whose patterns tend to become less distinct.

Acknowledgement

We acknowledge technical support by Dr. Takanobu Hiroto for XRD, and Mr. Taku Moronaga, Ms. Yuka Hara, and Ms. Akiko Nakamura for SEM-EBSD in Research Network and Facility Service Division in National Institute for Materials Science (NIMS).

REFERENCES

[1] S. Suzuki: Features of recent EBSD and its future, J. JILM **72** (2022) 570–577.
[2] N.C.K. Lassen, D.J. Jensen and K. Conradsen: Image Processing Procedures for Analysis of Electron Back Scattering Patterns, Scanning Microsc. **6** (1992) 115–121.
[3] S.I. Wright and B.L. Adams: Automatic analysis of electron backscatter diffraction patterns, Metall. Trans. A **23** (1992) 759–767.
[4] Q. Shi, D. Loisnard, Y. Li, Z. Chen, H. Wang and S. Roux: Accuracy assessment of crystal orientation indexations by EBSD, Meas. Sci. Technol. **35** (2024) 045030.
[5] R. Yoda, M. Kamaya, H. Kimura, T. Ohtani and K. Fujiyama: Round Robin Test Using EBSD for Creep Damage Evaluation, J. Soc. Mater. Sci., Japan **66** (2017) 130–137.
[6] K. Kubushiro, Y. Shioda and K. Nomura: Creep Degradation for Austenitic Stainless steel in KA-SUS304J1HTB, J. Soc. Mater. Sci., Japan **66** (2017) 179–184.
[7] S.-S. Rui, Y.-B. Shang, Y.-N. Fan, Q.-N. Han, L.-S. Niu, H.-J. Shi, K. Hashimoto and N. Komai: EBSD analysis of creep deformation induced grain lattice distortion: A new method for creep damage evaluation of austenitic stainless steels, Mater. Sci. Eng. A **733** (2018) 329–337.
[8] W.C. Lenthe, S. Singh and M. De Graef: A spherical harmonic transform approach to the indexing of electron back-scattered diffraction patterns, Ultramicroscopy **207** (2019) 112841.
[9] R. Hielscher, F. Bartel and T.B. Britton: Gazing at crystal balls: Electron backscatter diffraction pattern analysis and cross correlation on the sphere, Ultramicroscopy **207** (2019) 112836.
[10] KA-SUS 310J1 TB, The material specification in the Technical Regulation of Equipment for Thermal Power Plant, (2016).
[11] NIMS Creep Data Sheet, Metallographic Atras of Long-term Crept Materials, No. M-12, (2019).
[12] A. Winkelmann, C. Trager-Cowan, F. Sweeney, A.P. Day and P. Parbrook: Many-beam dynamical simulation of electron backscatter diffraction patterns, Ultramicroscopy **107** (2007) 414–421.
[13] P.G. Callahan and M. De Graef: Dynamical Electron Backscatter Diffraction Patterns. Part I: Pattern Simulations, Microsc. Microanal. **19** (2013) 1255–1265.
[14] J.B. Nelson and D.P. Riley: An experimental investigation of extrapolation methods in the derivation of accurate unit-cell dimensions of crystals, Proc. Phys. Soc. **57** (1945) 160–177.
[15] S. Suzuki: Principal of EBSD Method and Its Application to Microstructure Analysis of Materials, J. Japan Inst. Electron. Packag. **13** (2010) 469–474.
[16] W. Hume-Rothery, G.W. Mabbott and K.M.C. Evans: The freezing points, melting points, and solid solubility limits of the alloys of sliver and copper with the elements of the b sub-groups, Philos. Trans. R. Soc. London, Ser. A **233** (1934) 1–97.
[17] S. Suzuki: *EBSD Tokuhon =OIM-wo Shiyo suruni atatte= B 4.00*, (TSL Solutions, 2021).